ISSN 1330-3651(Print), ISSN 1848-6339 (Online)
https://doi.org/10.17559/TV-20240702001817
Original scientific paper

Research on Damage Identification of Beam Structure Based on Dynamics

Weishuo XU, Hao LI*, Cheng ZHANG, Junjiang LU, Baoxin QI

Abstract: In this article, the damage identification methods based on structural modes are discussed. According to the curvature modes before and after damage, the traditional structural damage location method based on curvature change is improved, and based on the vibration differential equation of Euler-Bernoulli beam and Perturbation theory established a quantitative identification method for small structural damage. The cantilever aluminum beam model is established by ABAQUS, and different damage conditions are set up. The damage index method (D-index) and the curvature damage factor method (CDF) are used for localization analysis, and the perturbation theory is used to introduce the damage parameter ε for quantitative analysis. Taking the cantilever aluminum beam as the test object, the Piezoelectric Transducer-Scanning Laser Doppler Vibrometer (PZT-SLDV) modal test system is used to conduct vibration tests to verify the rationality and applicability of the methods, discuss the damage location, damage relationship between parameters. The research shows that the damage location can be accurately identified by the damage index method and the damage factor method, and the small damage severity can be effectively quantified by the damage parameter.

Keywords: aluminum beam; curvature mode; damage detection; damage severity identification; dynamics; PZT-SLDV

1 INTRODUCTION

Structural health monitoring (SHM) techniques have been a focal point for scholars worldwide, with particular emphasis on vibration-based methods for structural damage identification due to their practicality, speed, and simplicity [1-4]. These approaches have garnered significant attention from the international academic and engineering communities. Vibration-based methods hold immense potential in resolving structural characteristics, especially in the realm of damage detection. The increasing robustness of SHM techniques also provides further opportunities for precise quantification and interpretation through vibration technologies [5, 6].

In 1991, Pandey et al. [7] made finite element analysis on a beam, calculated displacement mode, adopted central difference method to calculate curvature mode from displacement mode, and proved curvature mode as a good damage identification indicator. In 1999, Abdel et al. [8] studied the application of modal curvature change in pre-stressed concrete bridge detection. Simply supported beam and continuous beam containing damaged parts at different locations were tested using simulated data, while introducing a damage indicator called "curvature damage factor", and this technology was further applied to actual structures. A method of damage assessment is proposed by Lestari and Qiao et al. [9] based on the combination of numerical simulation of curvature vibration shape and experiment, established analytical relationship between damaged beams and healthy beams, and estimated damage severity according to the changes of structural dynamic characteristics determined by experiment. Qiao [10] verified the effectiveness of three damage detection algorithms, namely gapped smoothing method (GSM), generalized fractal dimension (GFD) and strain energy method (SEM), by using surface bonding piezoelectric sensor (PVDF) system and non-contact scanning laser vibrometer (SLV) system, and pointed out that all algorithms using uniform load surface (ULS) curvature curves can detect the presence and size of damage. Gupta et al. [11] employed Support Vector Machine (SVM) as a novel array technique, utilizing Laser Doppler Vibrometer (LDV) to extract the mode shapes of honeycomb sandwich structures. Through a combination of simulation and experimental approaches, they utilized Support Vector Classification and Regression Analysis, finding that the former yielded superior results in predicting delamination locations.

Poornima et al. [12] evaluated the damage detection capabilities of artificial neural networks (ANN) and support vector machines (SVM) in identifying damage in beams. The results indicated that both algorithms were accurate in detecting damage in cantilever beams, but the performance of ANN exceeded that of SVM. Altammar et al. [13] identified damage characteristics by combining the use of frequency response functions with optimization methods, probabilistically determining significant details such as damage location and severity. Randiligama et al. [14] utilized the combination of Absolute Change in Mode Shape Curvature (ACMSC) with Artificial Neural Network (ANN) to detect, localize, and quantify damage in hyperbolic cooling towers, successfully assessing the unknown severity of damage within the cooling towers. Sokhangou et al. [15] applied an improved method combining Modal Curvature Analysis and Wavelet Transform Curvature (WTC) to identify and highlight damaged areas in Ultra-High-Performance Fiber-Reinforced Concrete (UHPFRC) beams. By casting three 2-meter-span UHPFRC beams and artificially inducing damaged regions, as well as measuring free vibration responses, the study compared two damage identification methods: Damage Index (DI) and the WTC method. The results indicated that the WTC method, combined with modal curvature, could better identify damaged areas in UHPFRC beams.

Vibration analysis research finds extensive applications across various fields, from structural health monitoring to earthquake engineering, providing crucial insights to understand and enhance the performance of complex systems. With ongoing technological advancements, such as sensor technology and data processing algorithms, scholars both domestically and internationally have achieved significant research results in damage identification and assessment through vibration analysis. However, these efforts are constrained by the specific application scope and limitations of metrics [16, 17]. In vibration analysis, modal curvature serves as an effective indicator for studying damage. The primary objective of this study is to estimate the location of damage using the damage index method and damage factor method, assess the severity of damage through the mathematical relationship between curvature patterns and dynamic parameters, and explore the potential of damage detection in practical engineering applications using a PZT-SLDV measurement system.

2 THEORETICAL BACKGROUND

2.1 Vibration Theory

Based on the Euler-Bernoulli beam theory, an analytical relationship for the vibration of beam is established, and the equation of motion for the vibration of beam is expressed:

$$\frac{\partial^2}{\partial x^2}\left\{EI(x)\frac{\partial^2}{\partial x^2}\left[W(x,t)\right]\right\}+m(x)\frac{\partial^2}{\partial t^2}\left[W(x,t)\right]=0 \tag{1}$$

Of which: $EI(x)$ is the bending stiffness of beam; $m(x)$ is the mass distribution of beam per unit length along the x-axis direction; $W(x, t)$ is the displacement function of beam regarding position x and time t. Assuming its displacement function is:

$$W(x,t)=\phi(x)e^{j\sqrt{\lambda}t} \tag{2}$$

Then Eq. (1) can be rewritten as:

$$\frac{d^2}{dx^2}\left(EI(x)\frac{d^2}{dx^2}[\phi_i(x)]\right)-m(x)\lambda_i[\phi_i(x)]=0 \tag{3}$$

This paper only considers the stiffness loss caused by damage, but ignores the change of neutral axis caused by damage, as shown in Fig. 1. The distribution of flexural stiffness along the beam is a function that correlates to the location of the damage, the stiffness loss caused by damage is expressed as dimensionless parameter, and this stiffness loss parameter, as an indicator measuring the structural damage severity in this paper, denotes equivalent bending stiffness loss in the damaged region.

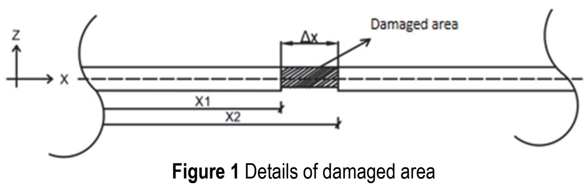

Figure 1 Details of damaged area

Assuming the stiffness loss parameter at the damage location is ε, then the influence of damage on the beam stiffness distribution can be expressed as:

$$EI_d(x)=EI_0\left\{1-\varepsilon\left[\mathbf{H}\left(x-x_1\right)-\mathbf{H}\left(x-x_2\right)\right]\right\} \tag{4}$$

In the Eq. (4), $\mathbf{H}$ represents Heaviside step function; EI_0 represents the bending stiffness of undamaged structure; x_1 and x_2 represent the boundary of damaged area. The governing equation of damaged beam can be expressed as:

$$\frac{d^2}{dx^2}\left\{EI_d(x)\frac{d^2}{dx^2}[\tilde{\phi}_i(x)]\right\}-\tilde{\lambda}_i m[\tilde{\phi}_i(x)]=0 \tag{5}$$

In the above equation, $\tilde{\phi}_i(x)$ and $\tilde{\lambda}_i$ are eigen functions and eigen values when the structure is in the damaged state. Assuming that the value of the damage size parameter "ε" is very small, the governing equation of damaged beam can be solved by using the perturbation method of beam in a complete state, and therefore the eigen solution of damaged structure can be represented by manner:

$$\begin{aligned}\tilde{\lambda}_i&=\lambda_i^0-\varepsilon\lambda_i^1-\varepsilon^2\lambda_i^2\\ \tilde{\phi}_i&=\phi_i^0-\varepsilon\phi_i^1-\varepsilon^2\phi_i^2\end{aligned} \tag{6}$$

By substituting Eq. (4) and Eq. (6) into Eq. (5), calculating only first order perturbation and retaining only first order calculation item, the structural curvature mode in the damaged state can be expressed through Eq. (7). Specific derivation steps are not presented here, and for the detailed steps, please refer to the article [7].

$$\begin{aligned}\tilde{\phi}_{i,xx}=\frac{d^2}{dx^2}\phi_i^0(x)-\varepsilon\Bigg[&\sum_{j=1}^{n}\frac{\lambda_i^0}{\lambda_i^0-\lambda_j^0}\{G_{1j}-G_{2j}+G_{3j}-G_{4j}-\\ &-G_{5j}\}\frac{d^2}{dx^2}\phi_j^0(x)-\left[\mathbf{H}\left(x-x_1\right)-\mathbf{H}\left(x-x_2\right)\right]\frac{d^2}{dx^2}\phi_i^0(x)\Bigg]\end{aligned} \tag{7}$$

The frequency of damaged beam $\tilde{\omega}$ can be expressed by the following equation:

$$\tilde{\omega}=\frac{\sqrt{\tilde{\lambda}_i}}{2\pi}=\frac{\lambda_i^0\left\{1-\varepsilon\left[G_{1j}-G_{2j}+G_{3j}-G_{4j}-G_{5j}\right]\right\}}{2\pi} \tag{8}$$

2.2 Damage Severity Quantification of Cantilever Beam

In case of damage in the structure, bending stiffness at the damaged place will decrease, and meanwhile, the size of curvature mode will change. The absolute value of the difference between curvature modes of healthy structure and damaged structure peaks within the damaged area, and is relatively small outside this area. Therefore, the curvature difference between order modes of healthy structure and damaged structure can be expressed as:

$$\Delta\phi_{i,j}^{"}=\left|\left\{\phi_h^{"}\right\}_{i,j}-\left\{\phi_d^{"}\right\}_{i,j}\right| \tag{10}$$

$$D_j=\sum_i\Delta\phi_{i,j}^{"} \tag{11}$$

$\phi_{i,j}^{"}$ represents the ith order curvature mode vibration shape of structure; the lower corner marks h and d represent that the structure is in the complete state and in the damaged state respectively; i represents mode number; j represents the location of measuring point on the beam surface. Curvature damage factor D_j is the sum of mode damage difference assessment. For the purpose of comparison and verification, damage index method

(D-index) [18] is also adopted, and this method is determined by the following expression:

$$\beta_{i,j}=\frac{\left\{\left(\phi_d^{"}\right)_{i,j}^{2}+\sum_{i=1}^{i\max}\left(\phi_d^{"}\right)_{i,j}^{2}\sum_{i=1}^{i\max}\left(\phi_h^{"}\right)_{i,j}^{2}\right\}}{\left\{\left(\phi_h^{"}\right)_{i,j}^{2}+\sum_{i=1}^{i\max}\left(\phi_h^{"}\right)_{i,j}^{2}\sum_{i=1}^{i\max}\left(\phi_d^{"}\right)_{i,j}^{2}\right\}} \tag{12}$$

$$\tilde{D}_j=\sum_i \beta_{i,j} \tag{13}$$

In the above equation, $\tilde{D}_j$ is the sum of damage index. Assuming that the presence of damage is determined at the x_d place, the damage level difference between healthy structure and damaged structure $\Delta\phi_{i,xx}(x_d)$ can be determined through the damage level difference between modes. This damage size or stiffness loss ε can be measured using the frequency relation or curvature relation. Because the frequency measurement under low frequency is rather sensitive to external interference, the estimation of damage size based on the relationship between curvature mode shapes and modal vibration. Assuming that the damage location x_d is known, the damage severity can be defined as:

$$\varepsilon=\frac{\phi_{i,xx}-\phi_{di,xx}}{\sum_{j=1}^{n}\frac{\lambda_i^0}{\lambda_i^0-\lambda_j^0}\left\{G_{1j}-G_{2j}+G_{3j}-G_{4j}-G_{5j}\right\}\frac{\mathrm{d}^2}{\mathrm{d}x^2}\phi_j^0(x)}- \\ -\left[\mathbf{H}(x-x_1)-\mathbf{H}(x-x_2)\right]\frac{\mathrm{d}^2}{\mathrm{d}x^2}\phi_i^0(x) \tag{14}$$

In the above equation, $\phi_{i,xx}$ and $\phi_{di,xx}$ represent the ith order curvature mode vibration shape of measured healthy and damaged structures respectively.

$$G_{1j}=\frac{\mathrm{d}}{\mathrm{d}x}\left[\phi_i^0(x_1)\right]\int_0^L < x-x_1 > \phi_j^0(x)\mathrm{d}x$$

$$G_{2j}=\frac{\mathrm{d}}{\mathrm{d}x}\left[\phi_i^0(x_2)\right]\int_0^L < x-x_2 > \phi_j^0(x)\mathrm{d}x$$

$$G_{3j}=\phi_i^0(x_1)\int_0^L \mathbf{H}(x-x_1)\phi_j^0(x)\mathrm{d}x$$

$$G_{4j}=\phi_i^0(x_2)\int_0^L \mathbf{H}(x-x_2)\phi_j^0(x)\mathrm{d}x$$

$$G_{5j}=\int_0^L\left[\mathbf{H}(x-x_1)-\mathbf{H}(x-x_2)\right]\phi_i^0(x)\phi_j^0(x)\mathrm{d}x$$

3 NUMERICAL SIMULATION

Based on the above analysis methods, the cutting damage assumption of cantilever aluminum beam is made, and numerical simulation is conducted. The component material used in simulation is standard aluminum, with elastic modulus of 6.9×10^4 MPa and density of 2.72×10^3 kg/m^3. The sectional dimension of designed beam is 25 mm wide, 20 mm high, and cantilever length is set as 500 mm. The front view of beam is shown in Fig. 2.

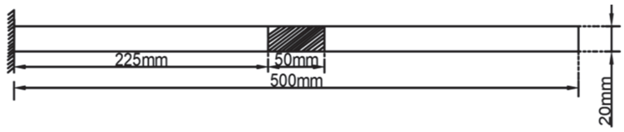

(a) Schematic diagram of front elevation

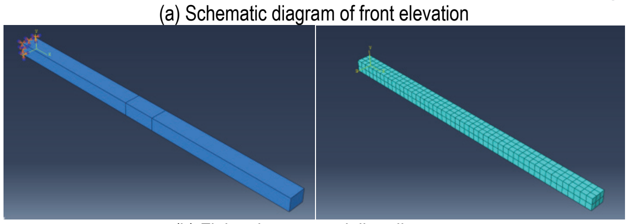

(b) Finite element modeling diagram

Figure 2 Schematic diagram of front elevation and Finite element modeling diagram of aluminum beam

Three kinds of damage conditions are assumed at 50% length position of the beam, with the same damage length of 50 mm, the damage severity at this place is expressed by stiffness reduction and when stiffness reductions are 0.1, 0.2, 0.3 respectively (ε = 0.1, 0.2, 0.3). ε = 0, it represents healthy aluminum beam. Under different stiffness loss assumptions, Eq. (7) and Eq. (8) are used to calculate natural frequency and curvature mode of beam. Tab. 1 shows the results of frequency change caused by damage under several damage situations, and Fig. 3 compares the curvature modes of healthy beam of the first four orders with those of the damaged aluminum beam under different stiffness losses.

As shown in Fig. 3, obvious difference occurs in different damage severity at the same damage locations. In Fig. 3a, Fig. 3b and Fig. 3d, curvature modes under different stiffness losses are significantly distinguished. Nevertheless, in Fig. 3c, when the damage location is in proximity to the node, the damage under this mode is less obvious for curvature. When the damage point is close to the node of a certain order vibration shape, curvature mode does not change significantly, indicating that curvature mode difference is not sensitive enough to the damage at the mode node [10]; considering that this reason may cause misleading results, the first four order curvature modes are used in damage assessment, rather than choose a single mode, so as to avoid the impact of damage location change on the results.

Table 1 The first four orders of natural frequency and percentage change

Orders	ε = 0	ε = 0.1		ε = 0.2		ε = 0.3	
	Frequency / Hz	Frequency / Hz	Change rate / %	Frequency / Hz	Change rate / %	Frequency / Hz	Change rate / %
1	63.96	63.9596	0.0006	63.9592	0.0012	63.9588	0.0018
2	397.93	397.94	−0.003	397.95	−0.005	397.96	−0.008
3	1101.6	1101.575	0.002	1101.55	0.005	1101.526	0.007
4	2124.2	2124.306	−0.005	2124.412	−0.01	2124.519	−0.015

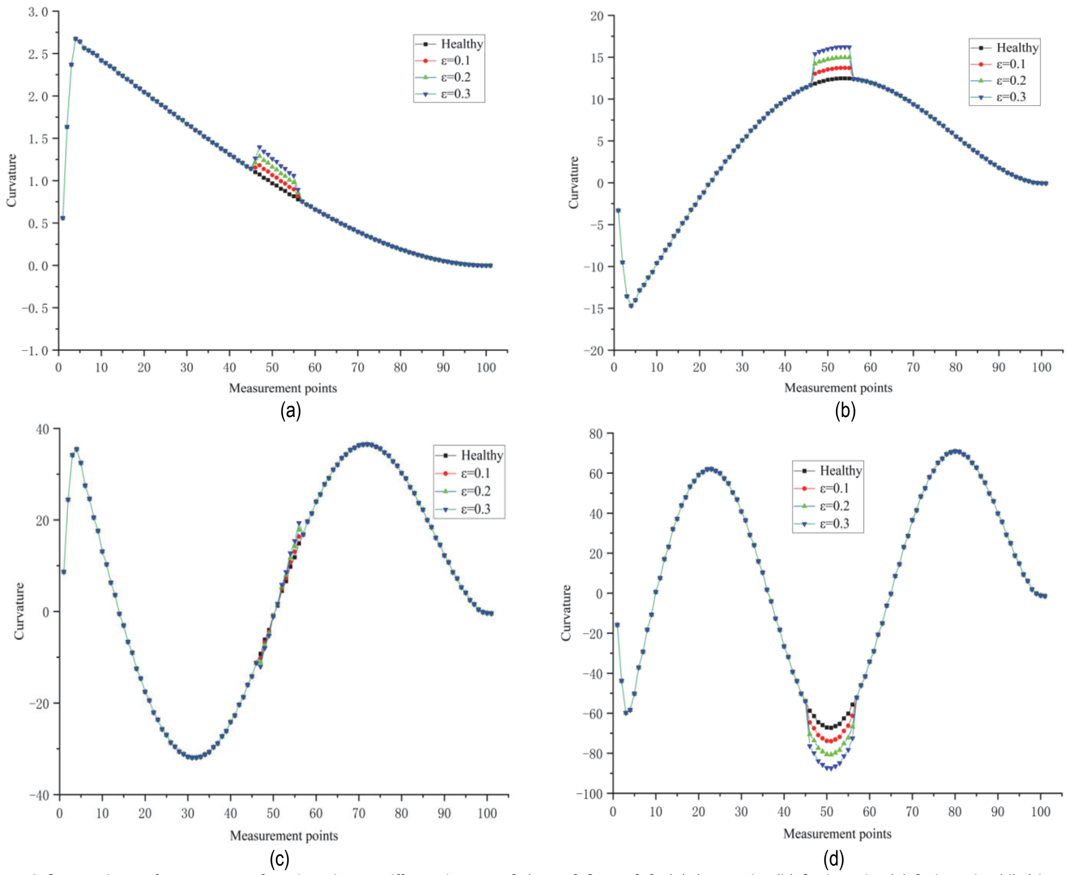

Figure 3 Comparison of curvatures of each order at stiffness loss ε = 0.1, ε = 0.2, ε = 0.3: (a) 1st mode; (b) 2nd mode; (c) 3rd mode; (d) 4th mode;

To study the applicability of this method, first of all, finite element modeling and analysis are performed using ABAQUS, and models of different damage severity at different damage locations are established using ABAQUS.

The size of calculation model is 600 mm × 25 mm × 20 mm, divided into 61 cells and 62 nodes along the length direction, with damage length of 50 mm and 5 cell lengths. See Fig. 4 for the schematic diagram of cell division.

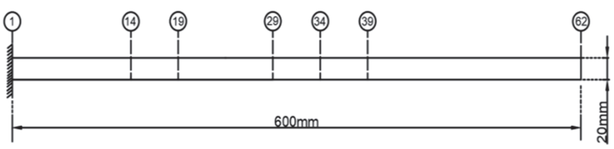

Figure 4 Schematic diagram of cell grid division

The cell damage is simulated by the reduction of elastic modulus, modal test data is obtained by finite element simulation of the structure, and damage parameters are calculated by using the obtained data. A total of three damaged components are established, each with different damage locations. The damage locations are set at nodes 14 - 19, nodes 29 - 34 and nodes 34 - 39 respectively, and then different stiffness reduction simulations are conducted at each damage location. Tab. 2 provides the specific configuration of damage.

Table 2 Damage location

Damage location	Damaged area / mm	Damage node
Location 1	125 - 175	14 - 19
Location 2	275 - 325	29 - 34
Location 3	325 - 375	34 - 39

According to simulation, the first four order vibration shapes under each stiffness reduction can be calculated, leading to beam frequencies at different locations after different stiffness reductions, as shown in Tab. 3. At the same location, the greater damage severity, the gradually less frequency.

Table 3 Frequency under different damage

Damage location	Damage severity / %	First order / Hz	Second order / Hz	Third order / Hz	Fourth order / Hz
No damage	0	44.957	280.3	778.69	1509
Location 1	5	44.786	280.22	776.49	1504.5
	15	44.393	280.05	771.51	1494.5
	25	43.91	279.84	765.52	1483
Location 2	5	44.91	279.09	778.52	1503.1
	15	44.803	276.3	778.11	1489.9
	25	44.668	272.92	777.6	1474.5
Location 3	5	44.932	279.13	777.24	1506.5
	15	44.874	276.44	773.95	1500.8
	25	44.802	273.15	770.02	1494

For damage parameter calculation, the obtained displacement data is normalized first, and then curvature mode of each order is obtained [19]. If the damage cell is known, damage parameters can be calculated using Eq. (11). As shown in Tab. 4, for damage at the same location, the calculated value of damage parameters will gradually increase with the increase of damage severity. Additionally, the calculation results of damage parameters are shown differently under the same damage severity, which indicates the calculation results affected by the damage location.

Table 4 Damage severity calculation

Damage severity / %	Location 1		Location 2		Location 3	
	Damage parameter calculation / %	Error / %	Damage parameter calculation / %	Error / %	Damage parameter calculation / %	Error / %
5	5	0	4.77	−4.6	4.69	−6.2
15	14.27	−4.87	15.52	3.47	15.71	4.73
25	25.56	2.24	29.83	16	29.58	18.32

4 TEST VERIFICATION
4.1 Data Acquisition

To further explore the applicability of the method, several different damage conditions are established on cantilever aluminum beam in this paper for damage identification. The size of component used is 700 mm × 25 mm × 20 mm, and through CNC machining of machine tool, cutting damage is artificially created on the lower surface of experimental part to simulate the damaged component. The effective length of test component is changed by changing the length of component clamped by the clamp fixture. Therefore, the aluminum beams in this test fall into two sizes, 500 mm × 25 mm × 20 mm and 600 mm × 25 mm × 20 mm, as shown in Fig. 5a: In the 500 mm long aluminum beam, set the damage with damage length of 50 mm at the location of 225 mm - 275 mm away from the fixed end, and the damage depths are 3 mm, 7 mm and 10 mm respectively. Lyapin [20] pointed out in the study that increasing the number of sensor locations can enhance the accuracy of damage localization. Porcu et al.[21] also emphasized in their study the significant role played by the density of the measurement grid in the accuracy of damage detection. Utilizing SLDV for laser scanning measurements, increasing the number of measurement points can further improve the precision of results. Therefore, in this study, the beam was divided into 48 sections longitudinally, with 49 measurement points along its length.

As shown in Fig. 5b and Fig. 5c, in the 600 mm long aluminum beam, divide the beam into 58 cells and 59 measuring points along the longitudinal direction of beam. Set the cutting damages with damage length of 50 mm and depths of 3 mm and 7 mm respectively at the location of 125 mm - 17 5mm and 325 mm - 375 mm away from the fixed end. The specific damage configurations are shown in Tab. 5.

Table 5 Experimental component conditions

Case No.	Beam	Damage location / mm	Damage node	Damage size
1	500 mm beam	225 - 275	22 - 27	50 mm × 3 mm
2	500 mm beam	225 - 275	22 - 27	50 mm × 7 mm
3	500 mm beam	225 - 275	22 - 27	50 mm × 10 mm
4	600 mm beam	125 - 175	12 - 17	50 mm × 3 mm
5	600 mm beam	125 - 175	12 - 17	50 mm × 7 mm
6	600 mm beam	325 - 375	32 - 37	50 mm × 3 mm
7	600 mm beam	325 - 375	32 - 37	50 mm × 7 mm

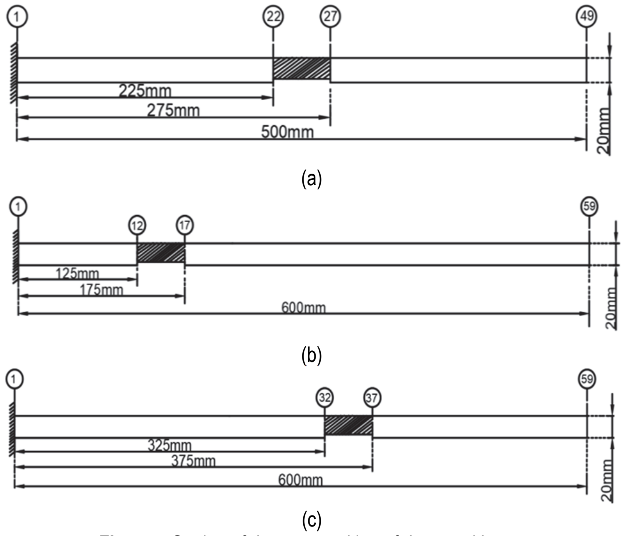

Figure 5 Setting of damage position of damaged beam

At the position near the fixed end of cantilever beam, paste a piece of 20 mm × 20 mm × 1 mm d33 piezoelectric ceramic plate (PZT for short) to the other side of the scanning surface using epoxy resin adhesive, and PZT functions as the excitation source in the vibration experiment [22]. Fig. 7a is a schematic diagram of the aluminum beams with PZT and the specific damage location. The test length of the cantilever beam is adjusted by adjusting the position of the member inserted into the fixture, and the attaching position of the PZT is adjusted to ensure that the excitation point of the member is near the fixed side of the cantilever beam. As shown in Fig. 7b, the signal arising from DG2052 signal generator is electrical signal, after the signal is amplified by the ATA-2032 high voltage amplifier and transmitted to PZT by using the soldering tin-connected wire, it is transferred into a force signal to excite the cantilever beam, and meanwhile, the PSV-500 Scanning Laser Doppler Vibrometer (SLDV for short) is used for data acquisition. The natural frequency and displacement mode data of cantilever beam are available through SLDV instrument, and these data are imported into MATLAB software for further analysis and processing of the data. Experimental process is shown in Fig. 6, and Fig. 7 is the test platform.

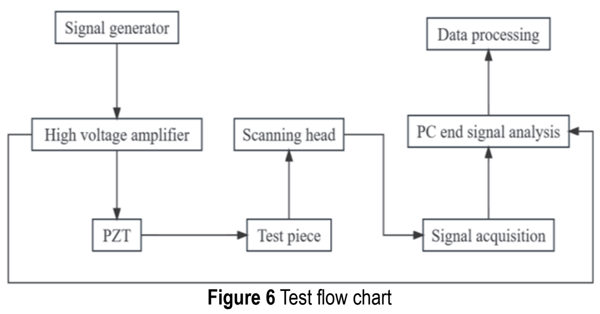

Figure 6 Test flow chart

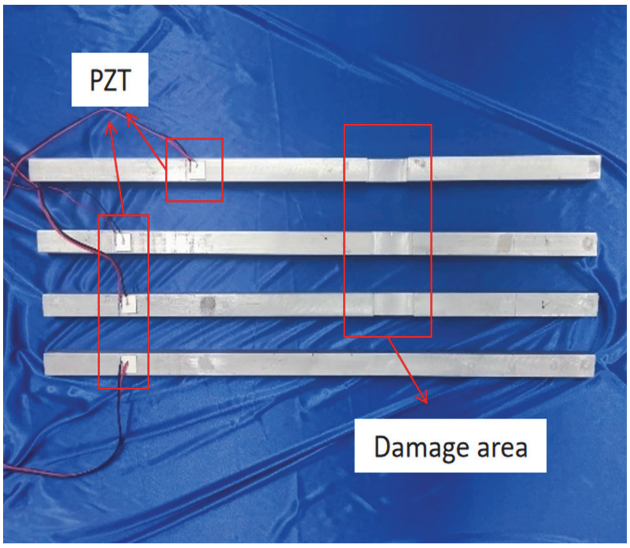

(a)

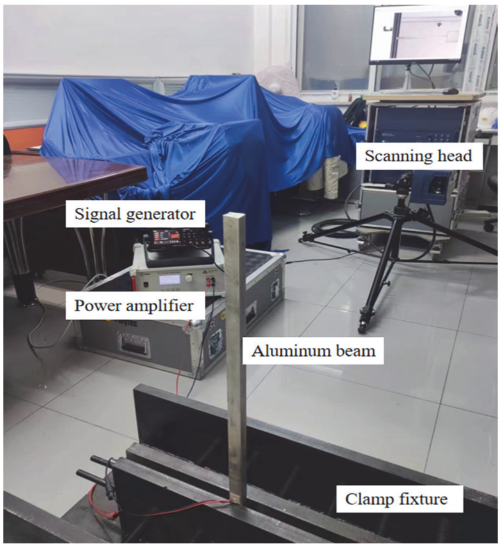

(b)

Figure 7 Experimental equipment: (a) Test specimens; (b) Test platform

First of all, regarding the function generator, select frequency sweeping wave as the excitation signal, and set the frequency sweeping range at 0 ~ 3000 Hz, frequency sweeping time at 1s and vibration amplitude at 10 Vpp. Amplify signal for 30 times through a high voltage amplifier. Deploy scanning points through the instrument SLDV, and for the 500 mm long aluminum beam test piece, divide the beam into 48 cells and 49 measuring points along the longitudinal direction of beam. For the 600 mm long aluminum beam test piece, divide the beam into 58 cells and 59 measuring points along the longitudinal direction of beam. Then complete setting of A/D parameter in SLDV before starting the test and information acquisition. After initial frequency sweep, cantilever beam will generate vibration frequency within the range of 0 ~ 3000 Hz after PZT excitation, and the actual natural frequencies of 1 - 4 orders of the cantilever beam in the experiment are available. Then, perform single frequency excitation of the sinusoidal signal of each order respectively, and adjust the average to 10 times, namely 10 times of vibration information acquisition conducted at each measuring point and the average results are taken as the final vibration information of this measuring point.

4.2 Experiment Results

After collecting and recording the measured data, conduct mode sorting and analysis of the data. Tab. 6 shows the frequencies under various cases. Cases 1 and 5 correspond to 500 mm healthy beam and 600 mm healthy beam respectively.

Table 6 Natural frequencies measured from experiments

Case No.	Damage depth / mm	First order / Hz	Second order / Hz	Third order / Hz	Fourth order / Hz
1	0	62.74	396.97	1107.18	2142.82
2	3	63.44	387.5	1123.44	1949.71
3	7	60.302	341.797	1099.12	1941.4
4	10	53.223	290.77	1047.12	1784.18
5	0	44.25	279.25	769.5	1475.75
6	3	42.25	281.25	756.5	1461.75
7	7	38.23	285.25	733.5	1430.75
8	3	43.25	267.25	752.5	1479.75
9	7	43.23	239.25	724.5	1432.75

After the displacement vibration shape of each order is obtained, import data into MATLAB to solve the curvature, as shown in Fig. 8 to Fig. 11 which illustrates the curvature mode of each order of the 500 mm long aluminum beam under different damage depths. The variations in modal shape curvature commonly exhibit discontinuities at damage sites, while also peaking significantly in the vicinity of the affected area. This observation aligns with the conclusions drawn by scholar Koushik Roy [23], providing further evidence of the abrupt changes in modal curvature at damaged regions. Such insights are pivotal for guiding future research efforts focused on curvature-related investigations. In Fig. 8a, under the case of 3 mm damage depth, curvature mode of damaged beam obviously varies from that of healthy beam at the damage place, and the curvature differences of the second and fourth order at the damage place are more obvious, nevertheless, under the third order mode, namely when damage is at the modal node, the damage at the depth of 3 mm is not obvious here, but more prominent at the depths of 7 mm and 10 mm. Fig. 12 shows the first four order curvature modes obtained under cases 6 and 7. It is visible that good indexes are presented for curvature modes, regardless of whether the damage depth is 3 mm or 7 mm. Fig. 13 shows the first four order curvature modes obtained under cases 8 and 9. As shown in Fig. 13a, under case 8, namely when the damage depth is 3 mm here, the damage location cannot be clearly identified, and the curvature change at the damage place is covered by noise, but in other modes, the curvature index presents good results. Noise has always been a major challenge for scholars both domestically and internationally [24, 25]. When conducting research under low-frequency conditions, scholars typically aim to work in an ideal noise-free environment or employ methods to mitigate noise pollution. However, in practical engineering scenarios, it is unrealistic to achieve a noise-free environment. Utilizing certain noise filtering methods may inadvertently weaken the accuracy of damage identification, failing to accurately reflect the actual severity of damage. Nevertheless, the method proposed in this study overcomes this limitation.

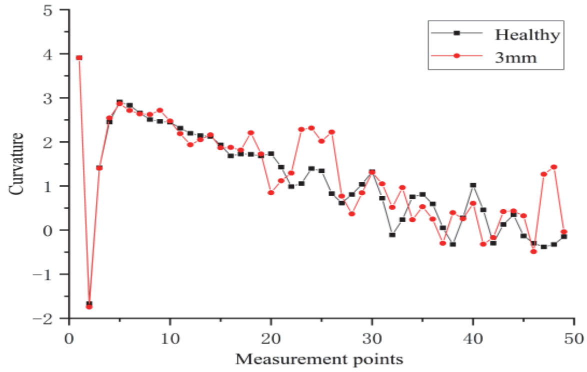

(a)

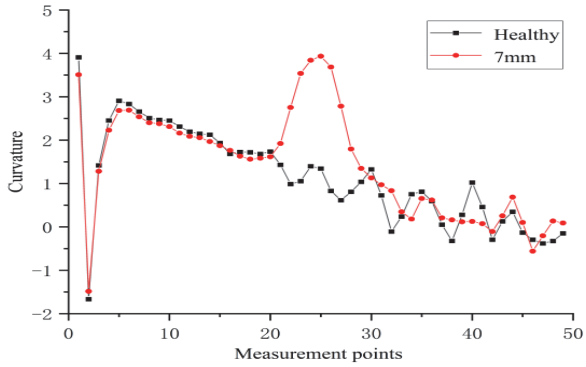

(b)

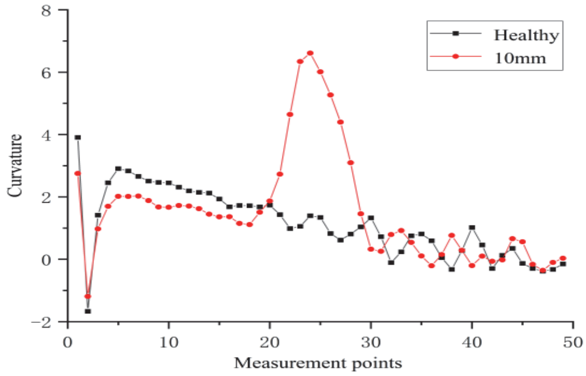

(c)

Figure 8 Comparison of first-order curvature mode shapes of damaged beam and healthy beam under case 2, 3 and 4: (a) Case 2; (b) Case 3; (c) Case 4

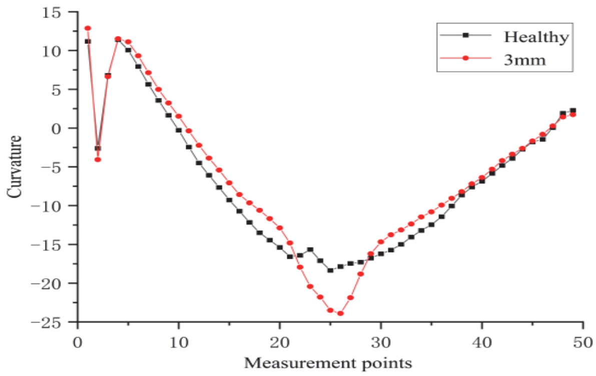

(a)

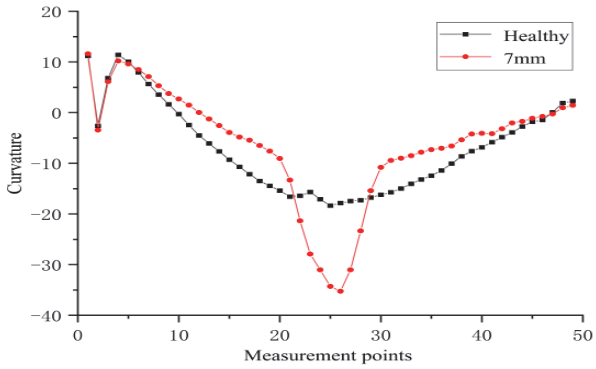

(b)

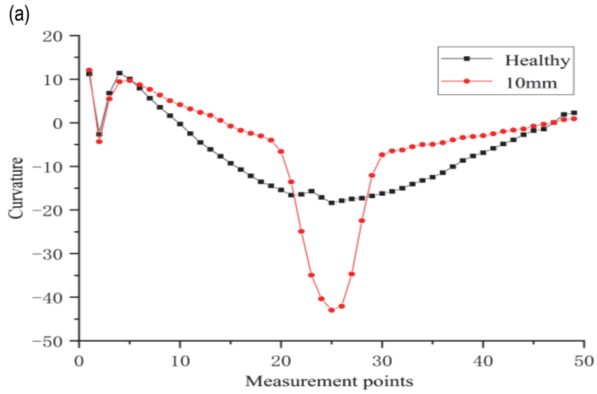

(c)

Figure 9 Comparison of second-order curvature mode shapes of damaged beam and healthy beam under case 2, 3 and 4: (a) Case 2; (b) Case 3; (c) Case 4

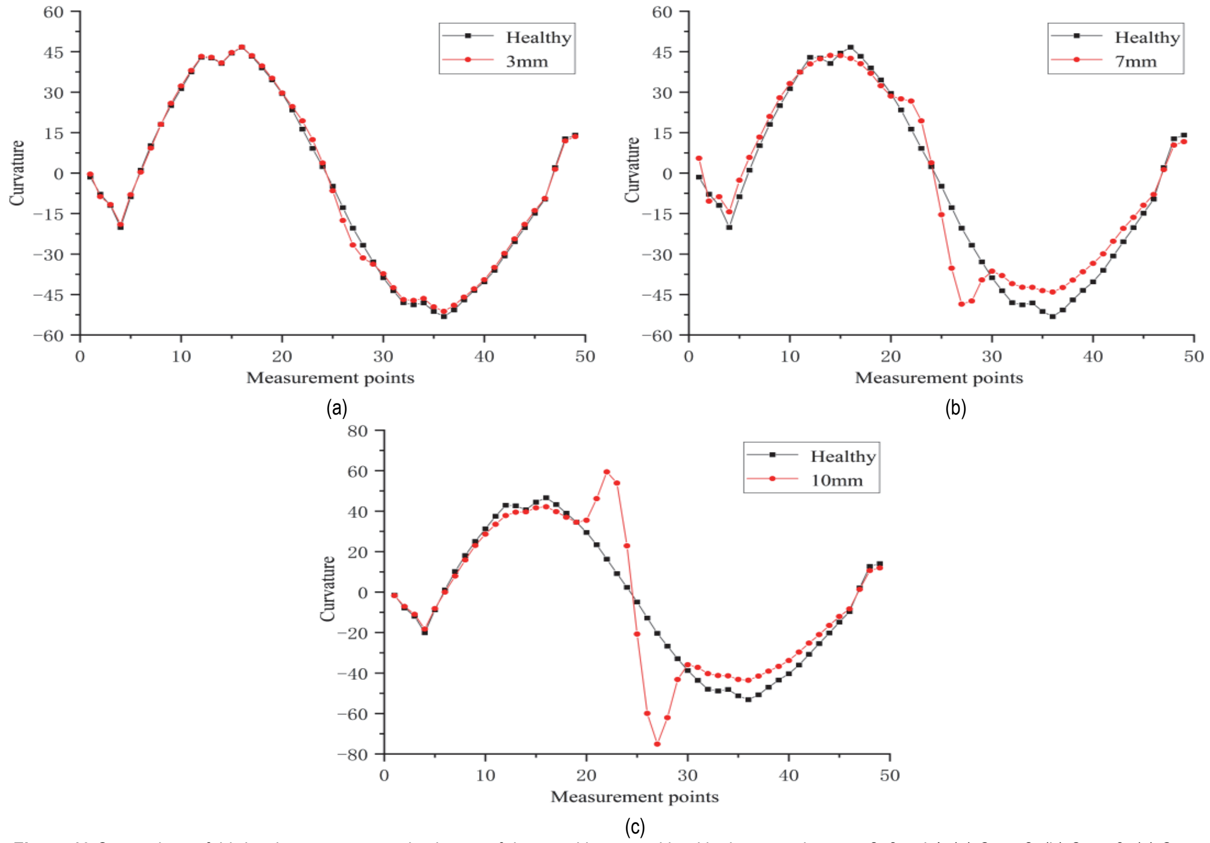

Figure 10 Comparison of third-order curvature mode shapes of damaged beam and healthy beam under case 2, 3and 4: (a) Case 2; (b) Case 3; (c) Case 4

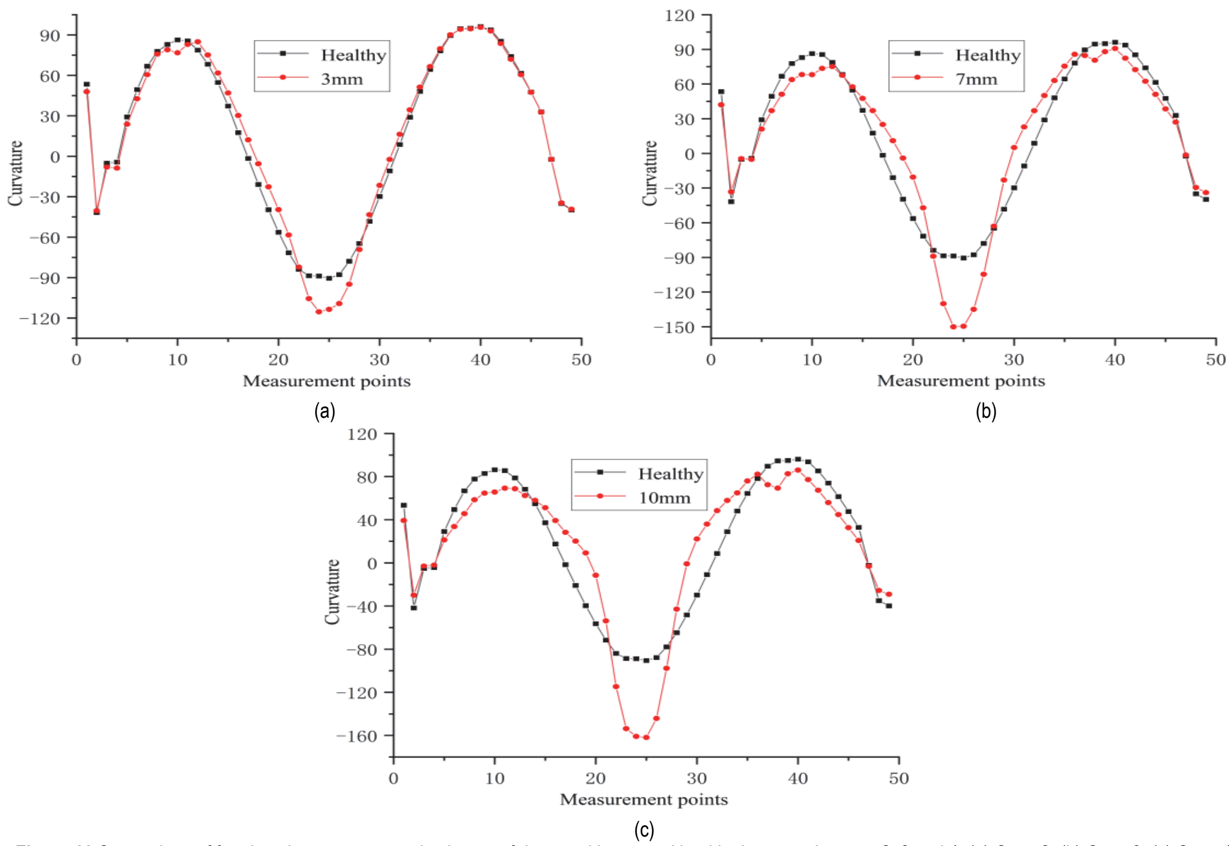

Figure 11 Comparison of fourth-order curvature mode shapes of damaged beam and healthy beam under case 2, 3 and 4: (a) Case 2; (b) Case 3; (c) Case 4

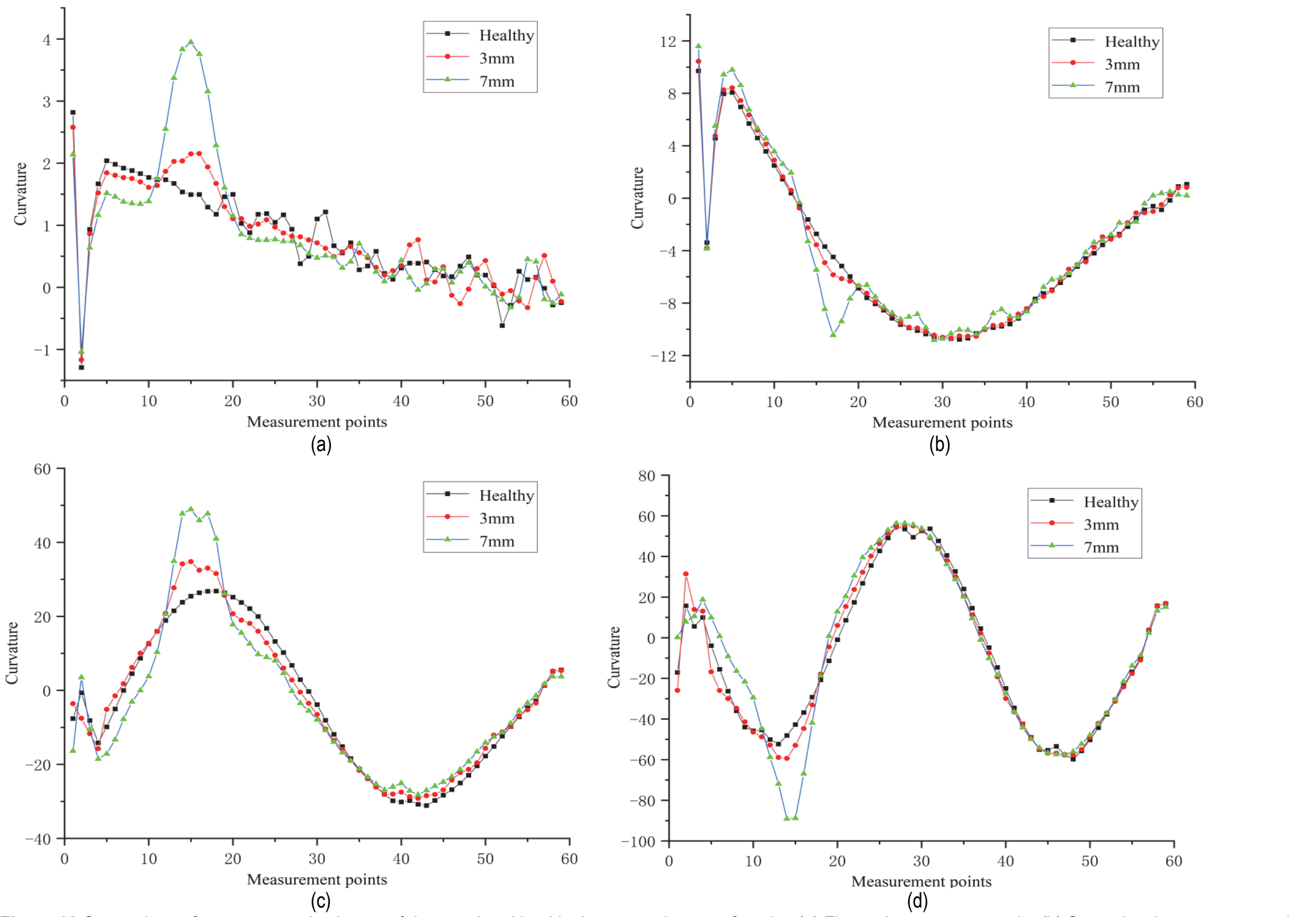

Figure 12 Comparison of curvature mode shapes of damaged and healthy beams under case 6 and 7: (a) First-order curvature mode; (b) Second-order curvature mode; (c) Third-order curvature mode; (d) Fourth-order curvature mode;

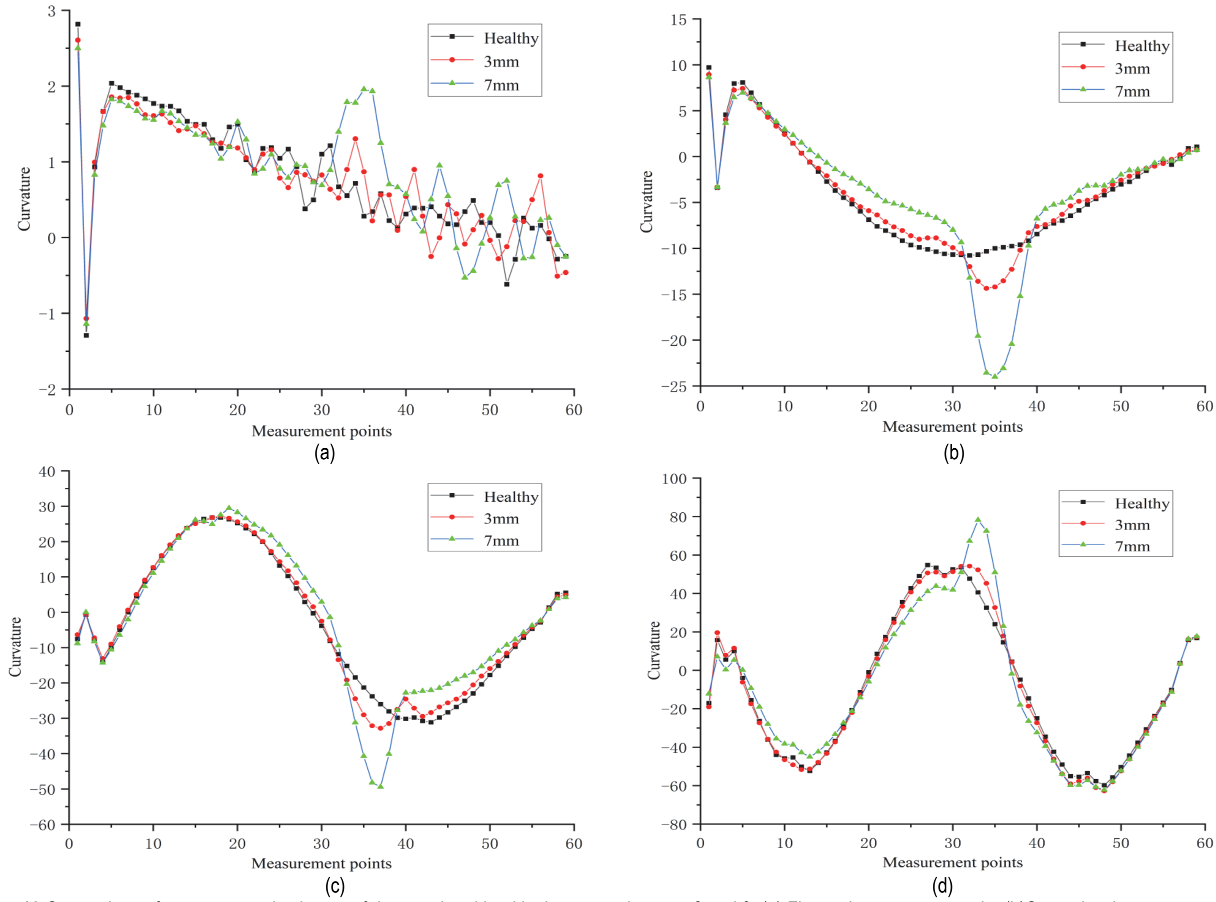

Figure 13 Comparison of curvature mode shapes of damaged and healthy beams under case 8 and 9: (a) First-order curvature mode; (b)Second-order curvature mode; (c) Third-order curvature mode; (d) Fourth-order curvature mode

4.3 Damage Identification

Fig. 13 shows a comparison of sweeping sinusoidal excitation curvature damage factor (CDF) and damage index (*D*-index) results. It is visible that the trends of damage identification by damage factor and damage index are basically the same. For cutting damage of different depths, no matter where the damage is located, damage factor method and damage index method give almost the same index. Tab. 7 summarizes the damage location prediction of the structure under sweeping sinusoidal excitation, and the location is given in the form of measuring point number. The potential of the Curvature Damage Factor (CDF) and the Damage Index (*D*-Index) in damage identification is once again validated here [26-28].

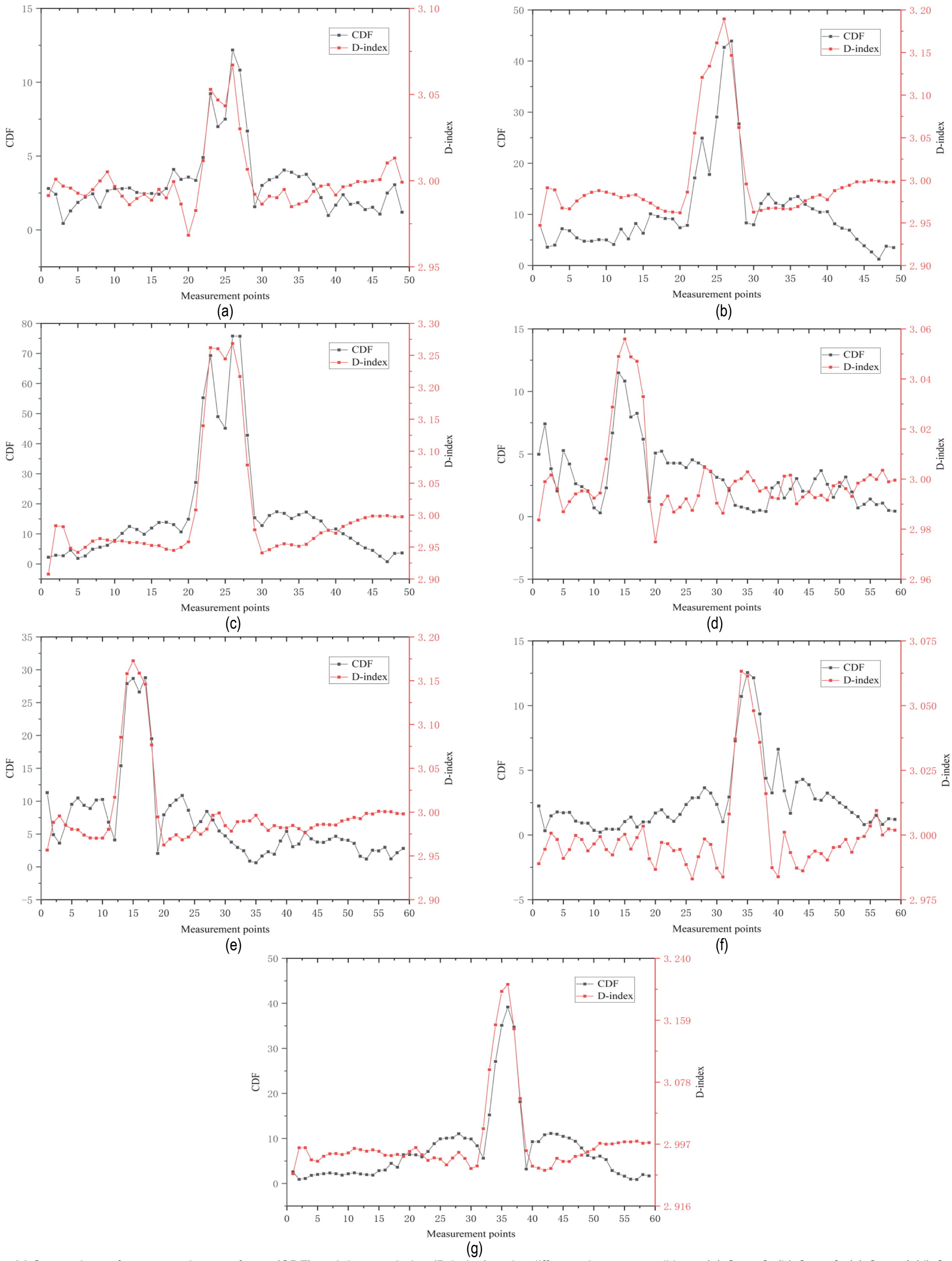

Figure 14 Comparison of curvature damage factor (CDF) and damage index (D-index) under different damage conditions: (a) Case 2; (b) Case 3; (c) Case 4 (d) Case 6; (e) Case 7; (f) Case 8; (g) Case 9

Table 7 Damage location estimation

Case No.	CDF	D-index	Actual damage location
2	22 - 28	22 - 28	22 - 27
3	22 - 28	22 - 28	
4	22 - 28	22 - 28	
6	12 - 18	13 - 18	12 - 17
7	12 - 18	12 - 18	
8	32 - 37	32 - 38	32 - 37
9	32 - 38	32 - 38	

4.4 Stiffness Loss Estimation

Predict the beam damage amplitudes under different damage conditions based on Eq. (11), and make assessment based on shape difference of each curvature mode. Fig. 12 compares the first four order curvature modes of aluminum beam under cases 6 and 7 with healthy beam; Fig. 13 compares the first four order curvature modes of aluminum beam under cases 8 and 9 with healthy beam; Fig. 15 compares the first four order curvature modes of aluminum beam under cases 2, 3 and 4 with healthy beam. Tab. 8 gives the calculated value of stiffness loss under various cases when the damage depth is 3mm, and damage can be predicted and estimated through Eq. (11). As shown in the table, when the damage depth is 3 mm, no matter where the damage is located, results are available through the equation to effectively quantify the damage.

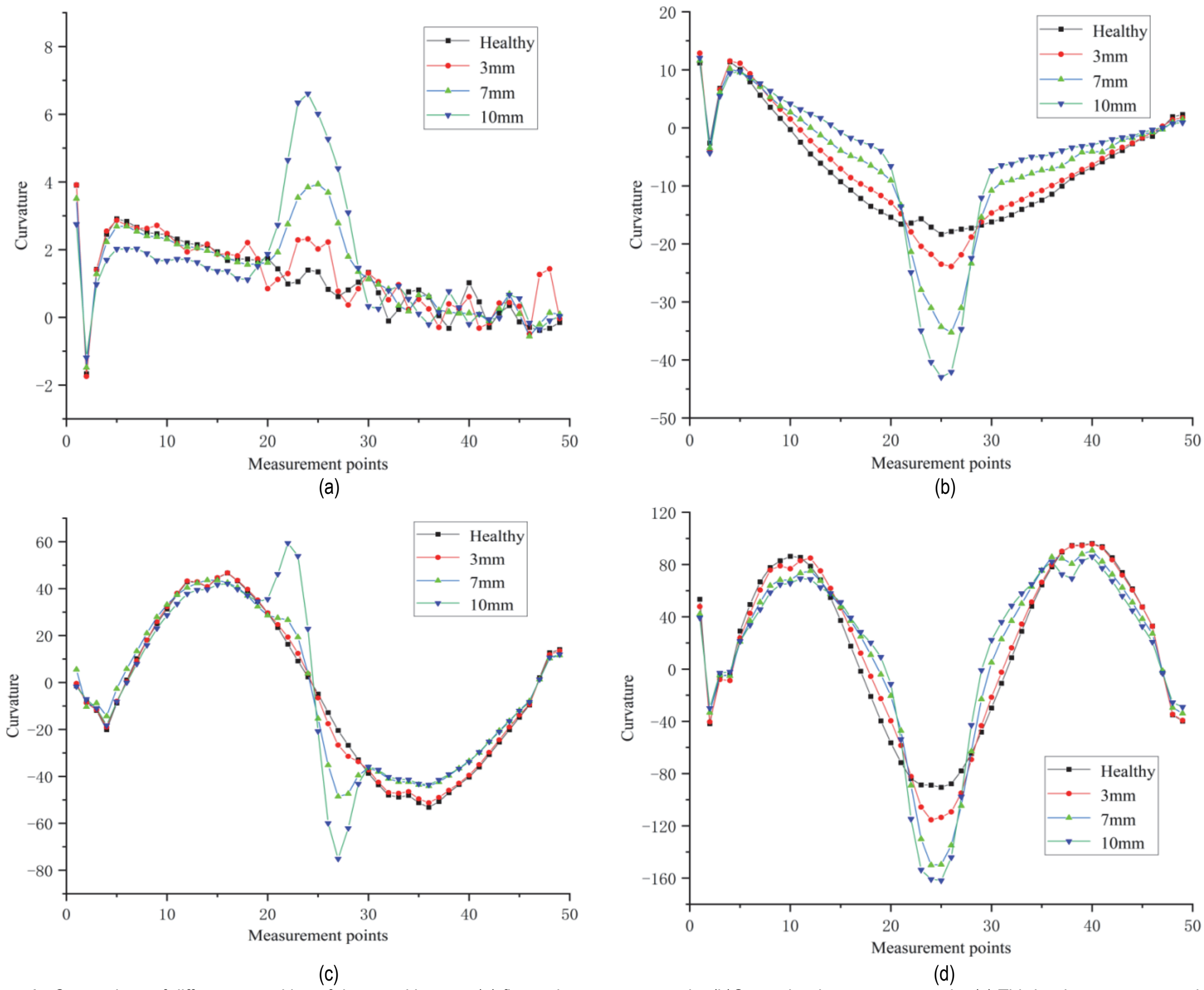

Figure 15 Comparison of different severities of damaged beams: (a) first order curvature mode; (b)Second order curvature mode; (c) Third order curvature mode; (d) Fourth order curvature mode

Table 8 Quantitative analysis of the severity of damage

Case No.	Theoretical stiffness loss / %	Calculated value of stiffness loss / %	Error / %
2	38.59	47.06	21.94
6	38.59	42.61	10.42
8	38.59	45.58	18.11

5 CONCLUSION

1. Using the PZT-SLDV measurement system for derivation of displacement vibration shape to obtain curvature and using damage factor method and damage index method for damage location detection, both methods are extremely sensitive to damage location identification and can accurately locate the damage.

2. Through numerical simulation, the damage factor calculation method can effectively identify and classify different damage degrees quantitatively.

3. Through finite element analysis and test verification, effective quantification analysis can be made on small damage. In actual engineering, when the damage location is determined, it can provide certain reference value for preliminary judgment of damage.

Acknowledgments

The work was supported by the Basic scientific research projects of colleges and universities in Liaoning Province (Project No. LJKMZ20220662); University of

Science and Technology Liaoning Youth Research Fund (Project No. 2020QN11)

6 REFERENCES

[1] Marques, D., Flor, F. R., Medeiros, R. D., Junior, C. D. C. P., & Tita, V. (2018). Structural Health Monitoring of Sandwich Structures Based on Dynamic Analysis.*Latin American Journal of Solids and Structures, 15*(3). e58, 1-22. https://doi.org/10.1590/1679-78254309

[2] Govindasamy, M., Kamalakannan., G., Kesavan, C., & Meenashisundaram, G. K. (2020). Damage Detection in Glass/Epoxy Laminated Composite Plates Using Modal Curvature for Structural Health Monitoring Applications. *Journal of Composites Science, 4*(4), 185-185. https://doi.org/10.3390/jcs4040185

[3] Nunes, L. A., Amaral, R. P. F., Barbosa, F. de S., & Cury, A. A. (2021). A hybrid learning strategy for structural damage detection. *Structural Health Monitoring, 20*(4), 2143-2160. https://doi.org/10.1177/1475921720966943

[4] Nguyen, Q. T. & Livaoğlu, R. (2023). Modal strain energy based enhanced approaches for damage detection and severity estimation. *Engineering Failure Analysis*, 146. https://doi.org/10.1016/j.engfailanal.2023.107142

[5] Moravvej, M. & El-Badry. M. (2024). Reference-Free Vibration-Based Damage Identification Techniques for Bridge Structural Health Monitoring-A Critical Review and Perspective. *Sensors, 24*(3). https://doi.org/10.3390/s24030876

[6] Azhar, A. S., Kudus, S. A., Jamadin, A., Mustaffa, N. K., & Sugiura, K. (2024). Recent vibration-based structural health monitoring on steel bridges: Systematic literature review. *Ain Shams Engineering Journal, 15*(3). https://doi.org/102501. 10.1016/j.asej.2023.102501

[7] Pandey, A. K., Biswas, M., & Samman, M. M. (1991). Damage detection from changes in curvature mode shapes. *Journal of Sound Vibration, 145*(2), 321-332. https://doi.org/10.1016/0022-460x(91)90595-b

[8] Abdel Wahab, M. M. & De Roeck, G. (1991). Damage detection in bridges using modal curvatures: application to a real damage scenario. *Journal of Sound and Vibration, 226*(2), 217-235. https://doi.org/10.1006/jsvi.1999.2295

[9] Lestari, W, Qiao, P. Z., & Hanagud S. (2007). Curvature Mode Shape-based Damage Assessment of Carbon/Epoxy Composite Beams. *Journal of Intelligent Material Systems & Structures, 18*(3), 189-208. https://doi.org/10.1177/1045389x06064355

[10] Qiao, P. Z., Lestari, W., Shah, M. G., & Wang, J. L. (2007). Dynamics-based Damage Detection of Composite Laminated Beams using Contact and Noncontact Measurement Sys-tems. *Journal of Composite Materials, 41*(10), 1217-1252. https://doi.org/10.1177/0021998306067306

[11] Gupta, S., Satpal, S. B., Banerjee S., & Guha, A. (2016). Vibration Based Health Monitoring of Honeycomb Core Sandwich Panels Using Support Vector Machine. *International Journal on Smart Sensing and Intelligent Systems, 9*(1), 215-232. https://doi.org/10.21307/ijssis-2017-867

[12] Poornima, V. & Lute, V. (2021). Damage integrity assessment for beams using structural health monitoring technique. *International Journal of Structural Engineering, 11*(4), 413-439. https://doi.org/10.1504/ijstructe.2021.10040138

[13] Reis, P. A., Iwasaki, K. M. K., Voltz, L. R., Cardoso, E. L., & Medeiros, R. D. (2022). Damage detection of composite beams using vibration response and artificial neural networks. *Proceedings of the Institution of Mechanical Engineers, Part L: Journal of Materials: Design and Applications, 236*(7), 1419-1430. https://doi.org/10.1177/14644207211041326

[14] Randiligama, S. M. C. M., Thambiratnam, D. P., Chan, T. H. T., & Fawzia, S. (2021). Damage assessment in hyperbolic cooling towers using mode shape curvature and artificial neural networks. *Engineering Failure Analysis,* 129. https://doi.org/10.1016/j.engfailanal.2021.105728

[15] Sokhangou, F., Sorelli, L., Chouinard, L., Dey, P., & Conciatori, D. (2024). Detecting Multiple Damages in UHPFRC Beams through Modal Curvature Analysis. *Sensors, 24*(3). https://doi.org/10.3390/s24030971

[16] Dahak, M., Touat, N., & Kharoubi, M. (2018). Damage detection in beam through change in measured frequency and undamaged curvature mode shape. *Inverse Prob-lems in Science & Engineering,* 1-26. https://doi.org/10.1080/17415977.2018.1442834

[17] Li, M. Y., Wu, Z. Y., Yang, H. F., & Yue, F. (2020). Localization and Degree of Damage Based on Relative Curvature Difference and Frequency Perturbation. *Acta Mechanica Solida Sinica: The Chinese Society of Theoretical and Applied Mechanics, 33*(4), 187-204. https://doi.org/10.1007/s10338-019-00138-y

[18] Stubbs, N., Kim, J. T., & Farrar, C. R. (1995). Field Verificat-ion of a Nondestructive Damage Localization and Severity Estimation Algorithm. *Proceedings of SPIE-The International Society for Optical Engin-eering, 2460*, 210.

[19] Chang, M., Kim, K. J., & Lee, J. (2019). Hierarchical neural network for damage detection using modal parameters. *Structural Engineering and Mechanics, 70*(4), 457-466.

[20] Lyapin, A. & Shatilov, Y. (2016). Vibration-based Damage Detection of the Reinforced Concrete Column. *Procedia Engineering, 150*(C), 1867-1871. https://doi.org/10.1016/j.proeng.2016.07.184

[21] Porcu, M. C., Patteri, D. M.,Melis, S., & Aymerich, F. (2019). Effectiveness of the FRF curvature technique for structural health monitoring. *Construction and Building Materials, 226*, 173-187. https://doi.org/10.1016/j.conbuildmat.2019.07.123

[22] Deevi, D. A., Naidu, A. S. K., & Rao, B. D. V. C. M. (2020). Optimal PZT transducer location for effective damage identification in thin fixed plate. *Advances in Materials and Processing Technologies, 6*(2), 311-323. https://doi.org/10.1080/2374068x.2020.1732157

[23] Roy, K. (2017). Structural Damage Identification Using Mode Shape Slope and Curvature. *Journal of Engineering Mechanics, 143*(9). https://doi.org/10.1061/(asce)em.1943-7889.0001305

[24] Ahmad, S., Waleed, A.,Virk, S. U., Muhammad, T. R., Aamish, S., & Nasir, A. (2019). Multiple damage detections in plate-like structures using curvature mode shapes and gapped smoothing method. *Advances in Mechanical Engineering, 11*(5). https://doi.org/10.1177/1687814019848921

[25] Ahmad, S., Waleed, A., Virk, U. S., Riaz, M. T., Sharjeel, A., & Ahmad, N. (2020). Damage detection in a fixed-fixed beam using natural frequency changes. *Vibroengineering PROCEDIA,* 2020, 3038-3043. https://doi.org/10.1177/1687814019848921

[26] Eraky, A., Anwar, M. A., Saad, A., & Abdo, A. (2015). Damage detection of flexural structural systems using damage index method Experimental. *Alexandria Engineering Journal, 54*(3), 497-507. https://doi.org/10.1016/j.aej.2015.05.015

[27] Sarangapani, G. & Ganguli, R. (2017). Detection of local matrix cracks in composite beam using modal data and modular radial basis neural networks. *ISSS Journal of Micro and Smart Systems, 6*(2), 127-140. https://doi.org/10.1007/s41683-017-0013-z

[28] Nick, H., Aziminejad, A., Hosseini, M. H., & Laknejadi, K. (2021). Damage identification in steel girder bridges using modal strain energy-based damage index method and artificial neural network.*Engineering Failure Analysis, 119*. https://doi.org/10.1016/j.engfailanal.2020.105010

Contact information:

Weishuo XU
School of Civil Engineering,
University of Science and Technology Liaoning,
Anshan, 114051, PR China

Hao LI
(Corresponding author)
School of Civil Engineering,
University of Science and Technology Liaoning,
Anshan, 114051, PR China
E-mail: lh13904180780@163.com

Cheng ZHANG
Liaoning Metallurgical Geological Exploration Research Institute Co,
Anshan, 114038, PR China

Junjiang LU
School of Civil Engineering,
Shenyang Jianzhu University,
110168, PR China

Baoxin QI
School of Civil Engineering,
Shenyang Jianzhu University,
110168, PR China